Cubic $Mg_xZn_{1-x}O$ wide band gap solid solutions synthesized at high pressures

2005 J. Phys.: Condens. Matter 17 3377

(http://iopscience.iop.org/0953-8984/17/21/030)

INSTITUTE OF PHYSICS PUBLISHING JOURNAL OF PHYSICS: CONDENSED MATTER

J. Phys.: Condens. Matter **17** (2005) 3377–3384 doi:10.1088/0953-8984/17/21/030

Cubic $Mg_xZn_{1-x}O$ wide band gap solid solutions synthesized at high pressures

A N Baranov[1,2], V L Solozhenko[1], C Chateau[1], G Bocquillon[1], J P Petitet[3], G N Panin[4], T W Kang[4], R V Shpanchenko[5], E V Antipov[5] and Y J Oh[2]

[1] LPMTM-CNRS, Institut Galilée, Université Paris Nord, 93430 Villetaneuse, France
[2] Korea Institute of Science and Technology, Seoul 130-650, Korea
[3] LIMHP-CNRS, Institut Galilée, Université Paris Nord, 93430, Villetaneuse, France
[4] Quantum-Functional Semiconductor Research Center, Dongguk University, 3-26 Pildong, Chunggu, Seoul 100-715, Korea
[5] Chemistry Department, Moscow State University, 119992 Moscow, Russia

E-mail: anba@kist.re.kr

Received 4 March 2005, in final form 14 April 2005
Published 13 May 2005
Online at stacks.iop.org/JPhysCM/17/3377

Abstract

Stable $Mg_xZn_{1-x}O$ solid solutions ($0.32 \leqslant x \leqslant 0.67$) with a rock salt structure were synthesized at temperatures higher than 700 °C and pressures above 5 GPa. The lattice parameters and the Mg/Zn ratio were determined by the Rietveld method from the powder x-ray diffraction data. Raman scattering studies confirmed the cubic structure. Cathodoluminescence spectra have shown blue-shifted luminescence as a result of the band gap widening of the solid solutions.

1. Introduction

Zinc oxide is a wide band gap semiconductor (3.37 eV) with large exciton binding energy (60 meV) [1]. ZnO with MgO ($E_g = 7.5$ eV) solid solutions and $Mg_xZn_{1-x}O$ (MZO)-based heterostructures have drawn global attention due to their potential application for room-temperature lasers and diodes in the visible and ultraviolet regions. The practical realization of a UV laser depends on the possibility to modulate the band gap while keeping the lattice constant as close as possible to the active layer [2]. $Mg_xZn_{1-x}O$ solid solutions allow tailoring of the direct band gap materials into extremely short wavelength regions. Numerous attempts to synthesize continuous wide band gap solid solutions by alloying ZnO with MgO have been reported [3–12].

At normal conditions the stable phase of ZnO has a hexagonal wurtzite structure while MgO has a cubic periclase structure. According to the phase diagram [13–15], the MgO–ZnO system is of eutectic type, characterized by an extensive solubility of ZnO in the periclase (MgO-rich) phase and by a restricted solubility of MgO in a zincite, though the limits of the solubility depend on the experimental conditions.

The application of non-equilibrium synthesis routes such as pulsed laser deposition [2, 3, 5, 12], metal-organic vapour-phase epitaxy [10], molecular beam epitaxy [11], or reactive electron beam evaporation [16] to the film growth as well as low-temperature decomposition of solution-processed precursors [17, 18] leads to extended (as compared with the MgO–ZnO equilibrium phase diagram) MZO solid solutions for both cubic and wurtzitic MZO. The band gap energy of MZO varies from 3.4 to 4.4 eV for the wurtzite phase and from 5 to 7.5 eV for the cubic phase. The higher values of the band gap for the cubic MZO films as well as the strong dependence on the MgO composition are favourable for band gap tailoring [9]. However, in many cases it has not been possible to fabricate stable single-phase MZO alloys with a band gap between 4 and 6 eV.

The wurtzite structure of ZnO is dictated by a strong preference of Zn for tetrahedral coordination. A reversible phase transformation from wurtzite (B4 phase) to rock salt (B1 phase) in ZnO at about 9 GPa was described earlier [19–25]. The phase boundary between the B4 and B1 phases has been determined as a straight line, P (GPa) $= 6.1 - 0.0012T$ (°C), [23] and as temperature independent at 6 GPa [24]. The pressure for the B4-to-B1 transition for ball-milled ZnO increases up to 15.1 GPa [25], while heat treatment at 15 GPa and 280 °C of the same ZnO yields a single-phase metastable rock salt zinc oxide after quenching [26]. ^{67}Zn-Mössbauer spectroscopy has revealed that at high pressures the wurtzite phase of ZnO is highly unstable even against small nonaxial lattice distortions [27]. The optical properties of rock salt and wurtzitic ZnO at high pressures were experimentally studied by photoluminescence [28], Raman [29], and absorption [30] spectroscopies and they have also been theoretically calculated [31]. The increase of band gap up to 3.5 eV for thin MZO films ($x < 0.13$) was determined by optical absorption measurements under high pressure [32].

Application of a high pressure and high temperature (HPHT) technique to the MgO–ZnO system should enable one to stabilize the rock salt phase, and to create MZO phases with the cubic structure in the whole concentration range of solid solutions, and to modulate the band gap of MZO alloys in the UV region. Here we report the HPHT synthesis and optical properties of $Mg_xZn_{1-x}O$ solid solutions with rock salt structure over a wide range of concentrations.

2. Experimental

0.5 M aqueous zinc nitrate (Aldrich) solution was precipitated by an excess amount of 2 M ammonium bicarbonate solution. The precipitate was washed with distilled water and dried at 320 °C in a vacuum furnace for 3–5 h. MgO was obtained by calcination of magnesium hydroxide carbonate $4MgCO_3Mg(OH)_25H_2O$ (Aldrich) at 1000 °C. Stoichiometric mixtures of Zn-containing precursor and MgO in a Mg/Zn molar ratio corresponding to $Mg_xZn_{1-x}O$ composition with $x = 0.68$, 0.5 and 0.32 were ball-milled in acetone using a planetary mill, dried and afterwards annealed at 550 °C for 24 h. The morphologies and size distributions of the ZnO and MgO particles of the precursors were examined by high resolution transmission electron microscopy (HRTEM) using a JEM-4010 with accelerated voltage of 400 kV.

The high-pressure experiments at 5 GPa were carried out using a belt-type apparatus, while experiments up to 10 GPa were performed in a cubic multianvil press. As-prepared ZnO–MgO mixtures were uniaxially pressed into discs and placed into a high-pressure pyrophyllite cell with a graphite heater. The temperature was measured using a Pt10% Rh–Pt thermocouple without corrections for the pressure effect on the thermocouple emf. Sample pressure as a function of hydraulic oil pressure was calibrated using the known phase transitions in bismuth and barium, namely Bi_{I-II} (at 2.54 GPa), Ba_{II-III} (at 5.5 GPa) and Bi_{VI-VII} (at 7.7 GPa) at room temperature.

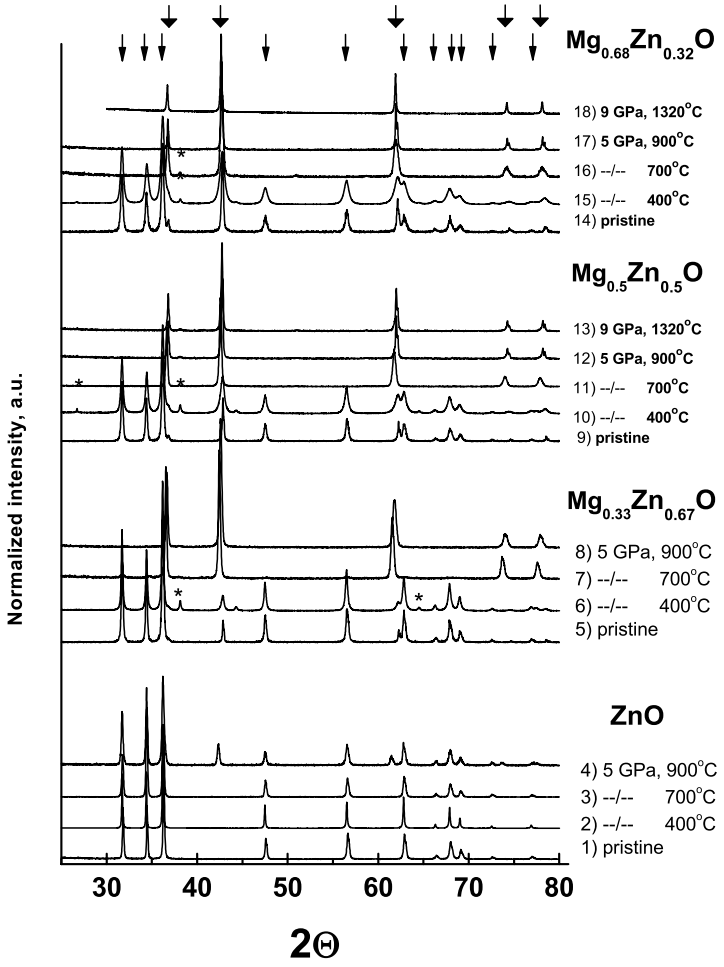

Figure 1. Powder x-ray diffraction patterns of $Mg_xZn_{1-x}O$ samples quenched from high pressures and temperatures and annealed at ambient pressure. Wide arrows denote peaks of the rock salt phase and narrow ones correspond to the wurtzite phase; asterisks denote impurity.

Quenched samples were studied by powder x-ray diffraction (XRD) using a Rigaku diffractometer (Cu Kα radiation). The diffraction experiment for structure refinement was carried out using a Huber G670 image plate Guinier camera (Cu Kα_1 radiation, curved Ge monochromator). The GSAS program [33, 34] was used for structure refinement by the Rietveld method. The occupation of the Zn/Mg positions was refined with fixed displacement parameters. The atomic coordinates for $Mg(OH)_2$ which appears occasionally as an impurity were taken from [35], and were not refined.

Cathodoluminescence (CL) spectra of the samples were obtained using an XL 30S FEG high-resolution scanning electron microscope (HRSEM) with a MonoCL system for CL spectroscopy. Micro-Raman spectra were recorded in backscattering configuration on an XY multichannel Jobin–Yvon spectrometer equipped with a CCD detector. The 514.5 nm line of the coherent Spectra-Physics argon-ion laser was used as the excitation source. A Leitz UT40 optical microscope was used to focus the laser on the sample and to collect the scattered signal.

3. Results and discussion

Figure 1 shows the x-ray diffraction patterns of the $Mg_xZn_{1-x}O$ samples quenched from high pressures and temperatures and annealed at ambient pressure. The peak positions in the XRD

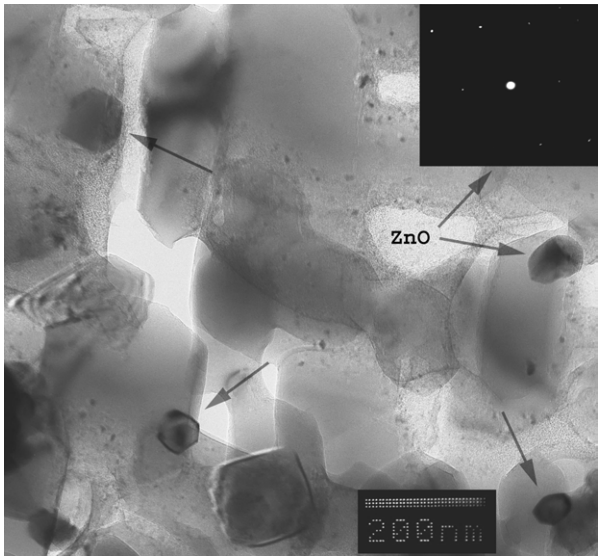

Figure 2. HRTEM image of the $Mg_{0.5}Zn_{0.5}O$ precursor. Inset: selected area electron diffraction pattern.

patterns taken from the pristine samples (patterns 1, 5, 9, and 14) correspond to ZnO (space group $P6_3/mc$ (186); ICDD PDF2 card 36-1451) and MgO (space group $Fm3m$ (225); ICDD PDF2 card 45-0946). No other peaks have been detected. This shows that the precursors contained only two pure oxides and did not form any solid solution because the temperature of the preliminary annealing (550 °C) was not high enough to produce a reaction. MgO/ZnO mixed nanoparticles prepared by solution techniques form the alloy with MZO near-band-edge emission at higher temperatures [36]. The HRTEM image for the MgO(68%)–ZnO(32%) precursor shows individual ZnO (denoted by arrows) and MgO particles (figure 2). They are well crystalline and single phase, as can be seen in the selected area electron diffraction pattern taken from a ZnO particle (inset in figure 2). The size of the particles is in the range 200–500 nm and 40–60 nm for MgO and ZnO, respectively.

The synthesis at 5 GPa and 400 °C did not result in the formation of a cubic phase, and the line positions have changed only slightly (figure 1, patterns 2, 6, 10, 15). The MZO samples quenched from 5 GPa and temperatures above 700 °C have a rock salt structure; lines of the hexagonal phase completely disappear in figure 1, patterns 7, 11, 16, which is in accordance with the phase diagram of ZnO [23, 24]. Earlier it has been reported that the pure B1 phase of ZnO is unquenchable, and all quenched ZnO samples contain either pure B4 phase or a mixture of B4 and B1 phases [19, 22, 23]. In our experiments at 900 °C and 5 GPa, wurtzitic ZnO transforms into a mixture of B1 and B4 phases (figure 1, pattern 4) whereas at 700 °C and 5 GPa, only hexagonal phase is detected (figure 1, pattern 3). MgO helps to stabilize the transformation of ZnO at high pressures and plays the role of 'substrate', keeping the rock salt structure after pressure release. One should note that XRD patterns 6, 10, 15, and 16 additionally exhibit weak peaks ($I < 2\%$) of $Mg(OH)_2$. The traces of magnesium hydroxide are possible due to reaction of initial MgO with air moisture during sample preparation.

The main results of the structure refinement are listed in table 1. The experimental and calculated XRD patterns and curve difference for the $Mg_{0.68}Zn_{0.32}O$ sample quenched from 700 °C and 5 GPa (A) and 1320 °C and 9 GPa (B) are shown in figure 3. The refinement of the pattern of sample 1 (figure 3(A)) revealed the formation of two solid solutions with different compositions but with the same rock salt structure. Although the $Mg_{0.5}Zn_{0.5}O$ sample (700 °C,

Table 1. Results of the Rietveld refinement for the $Mg_{1-x}Zn_xO$ compositions.

Number	Sample	*P–T* conditions	*a* (Å)	Mg:Zn	Formula weight	*V* (Å^3)	R_P, R_{wP}
1	$Mg_{0.68}Zn_{0.32}O$[a]	5 GPa, 700 °C	4.2440(2) 4.2291(2)	0.523(3):0.477(3) 0.889(4):0.111(4)	238.993 181.719	76.44(1) 75.64(1)	0.017, 0.012
2	$Mg_{0.5}Zn_{0.5}O$[b]	5 GPa, 700 °C	4.2500(1)	0.493(1):0.507(1)	244.533	76.768(7)	0.025, 0.017
3	$Mg_{0.68}Zn_{0.32}O$	9 GPa, 1320 °C	4.2356(6)	0.678(1):0.322(1)	214.128	75.991(1)	0.017, 0.011

[a] Phase 1:phase 2:$Mg(OH)_2$ ratio (wt%) is 55.8(1):39.8(2):4.4(1).
[b] Phase 1:$Mg(OH)_2$ ratio (wt%) is 97.7(1):2.3(1).

5 GPa) has been refined as a single-phase one, the scrutinizing of the peak shape at high angles points to the possible existence of a second rock salt phase. The sample with the $Mg_{0.68}Zn_{0.32}O$ starting composition treated at higher pressures and temperatures (9 GPa, 1320 °C) is a single phase, and has the rock salt structure. Due to the significant difference in scattering power of Mg and Zn cations, the refined values of occupancy factor are reliable, and agree very well with the tendency of variation of lattice constant of the rock salt-type solid solution caused by replacement of Mg by Zn. The lattice parameters for samples 1–3 lie between the values of $a_{MgO} = 4.2112$ Å, and $a_{cZnO} = 4.283$ Å reported in the literature [22].

The results of Raman spectroscopy measurements are shown in figure 4. Spectrum B taken from the ZnO sample quenched from 5 GPa and 400 °C shows Raman bands, typical for the ZnO. The bands at 94 and 430 nm^{-1} may be ascribed to E_2 (low) and E_2 (high) modes. A_1 bands at 373 and 576 nm^{-1} are also present in the spectrum but they are less pronounced [29]. Other bands may have originated from the multi-phonon processes [17]. Spectrum A taken from $Mg_{0.5}Zn_{0.5}O$ sample quenched from 5 GPa and 400 °C is similar to spectrum B. As follows from the XRD data (figure 1, pattern 10), the pressure is not sufficient for the phase transition while the temperature is not sufficient for the formation of solid solution; hence, we do not observe any substantial shift of Raman bands for the ZnO phase in spectrum A in comparison with spectrum B. In spectra C and D taken from the $Mg_{0.5}Zn_{0.5}O$ sample (1320 °C, 9 GPa) and $Mg_{0.68}Zn_{0.32}O$ sample (1320 °C, 9 GPa), respectively, the E_2 and A_1 Raman bands have disappeared, in accordance with the rule that first-order Raman scattering is forbidden for the rock salt structure. However, in the case of $Mg_xZn_{1-x}O$ solid solutions translation symmetry as well as inversion symmetry is destroyed by introducing Zn atoms at the substitutional lattice site, and first-order Raman scattering is allowed [37]. Nevertheless the 102 and 112 nm^{-1} bands remain and new broad features at 340 and 550 nm^{-1} appear. The latter can be explained by the presence of structural defects, for instance, anion vacancies. XRD is not sufficiently sensitive to study oxygen deficiency in the ZnO structure because of the small atomic scattering factor of oxygen. An additional neutron diffraction study is necessary to confirm the suggestion.

Figure 5 shows CL spectra obtained from the samples quenched from high pressures and high temperatures. The spectra do not exhibit the deep UV luminescence related with pure MgO. The near band gap luminescence of the solid solution is blue-shifted as the MgO concentration increases. Peaks centred at 3.55 and 3.74 eV are observed for the $Mg_{0.5}Zn_{0.5}O$ and $Mg_{0.68}Zn_{0.32}O$ quenched from 1320 °C and 9 GPa, respectively. In addition, the spectra of the quenched samples usually show a defect-related peak at about 2.2 eV. Despite the numerous reports on the photoluminescence and cathodoluminescence of ZnO, the luminescent centre responsible for this emission is not yet clearly identified. Several assumptions have been made. According to Vanheusden [38] and Egelhaaf [39], the peak corresponds to a defect-related

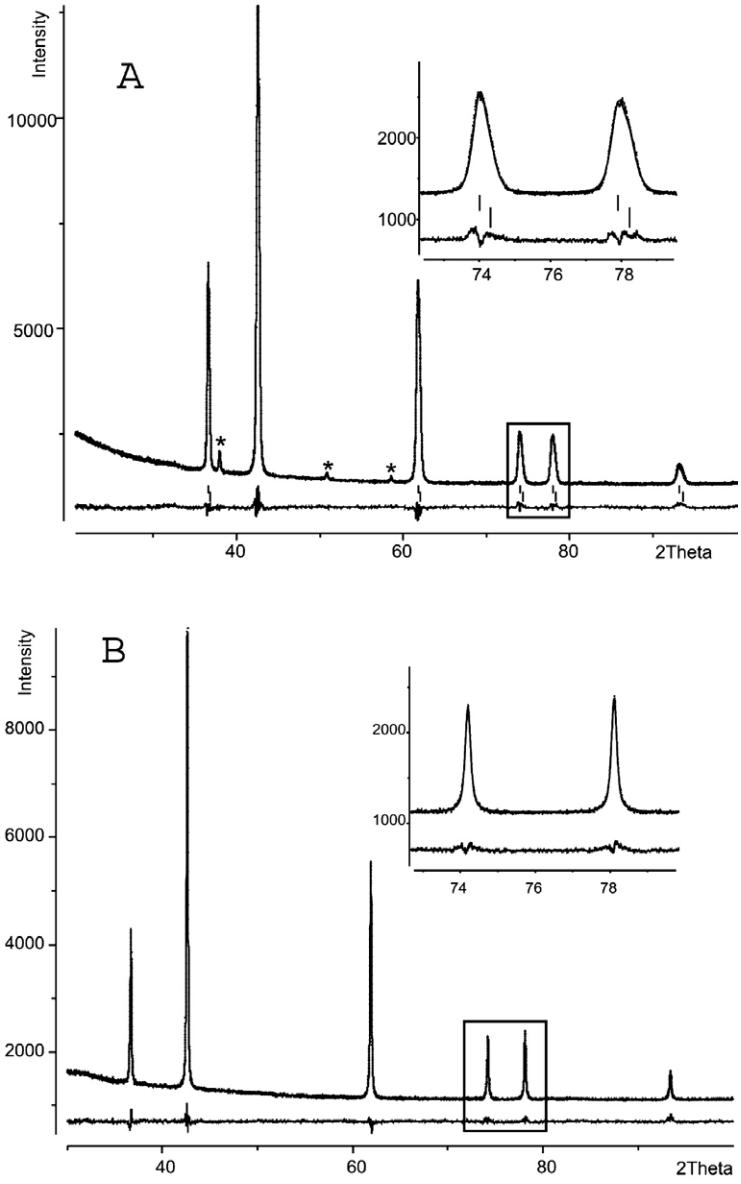

Figure 3. Refined XRD spectra of $Mg_{0.68}Zn_{0.32}O$ samples 1 (top) and 3 (bottom). Peak positions for two solid solutions are shown for sample 1 (part (A)) and peaks of $Mg(OH)_2$ are marked by asterisks. Enlargements demonstrate asymmetric broadening due to a presence of two cubic phases for sample 1 and single cubic phase for sample 3 (part (B)).

luminescence (deep-level luminescence) due to the oxygen vacancies in the ZnO crystal lattice. This defect-related luminescence is caused by radiative transitions between shallow donors (oxygen vacancies) and deep acceptors (zinc vacancies). Earlier, Chen [9] explained the broad transition in the experimental transmission spectra of cubic $Mg_xZn_{1-x}O$ by compositional non-uniformity. This approach allowed the experimental results to be brought into better agreement with theoretical ones. In our case, non-uniformity in x for $Mg_xZn_{1-x}O$ compositions could not

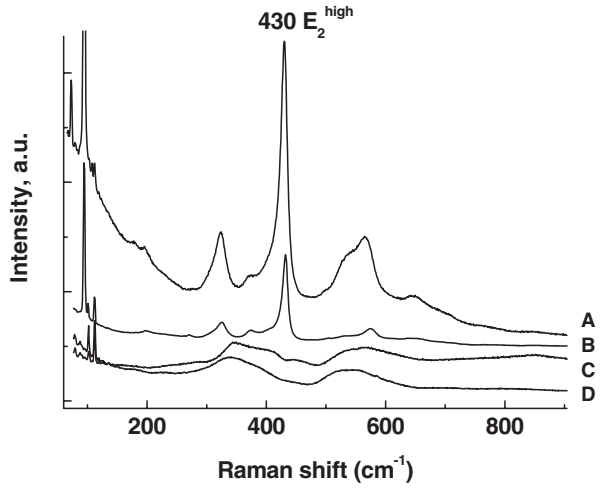

Figure 4. Raman spectra of $Mg_xZn_{1-x}O$ samples synthesized at 5 GPa and 400 °C (A) $x = 0.5$; (B) $x = 0$ and 9 GPa and 1320 °C (C) $x = 0.5$; (D) $x = 0.68$. The spectra are shifted for clarity.

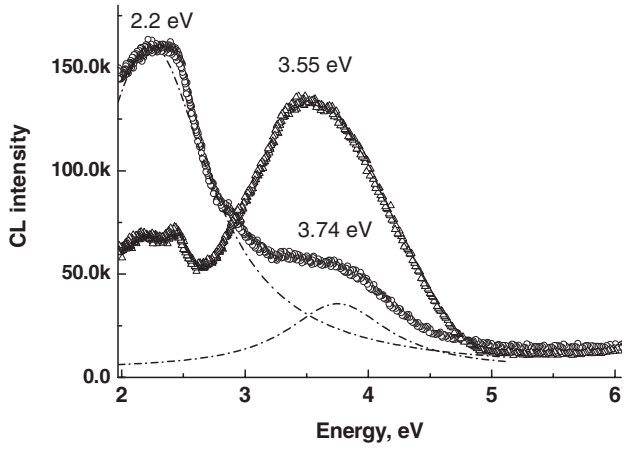

Figure 5. Cathodoluminescence spectra of $Mg_xZn_{1-x}O$ samples synthesized at 9 GPa and 1320 °C of different compositions: triangles—$x = 0.5$; circles $x = 0.68$ (dash–dot lines are Lorentz multi-fit approximations).

explain such broadness in the spectra, since the structure refinement for the studied samples has revealed the phase purity but the spectra are also broadened. One may suggest that non-uniformity is not in the phase homogeneity but in the distribution of structural defects like dislocations or oxygen vacancies, inside the phases. This explains why the values 3.55 and 3.74 eV obtained for our samples are considerably lower than the values determined for rock salt films with the same Mg composition [16, 40].

4. Conclusion

As a result of the present study, stable cubic $Mg_xZn_{1-x}O$ solid solutions ($0.33 < x < 0.68$) with continuous band gap up to 3.74 eV have been synthesized under high pressures and temperatures. The lattice parameters and the Mg/Zn ratio were determined by the Rietveld method from powder x-ray diffraction data. The optical properties of the quenched samples were characterized by CL and Raman spectroscopy. The blue shift in the luminescence spectra results from the band gap widening of the MZO solid solutions.

Acknowledgments

The authors thank O O Kurakevych for assistance in the high-pressure experiments. ANB has been receiving support from the Université Paris Nord, which is acknowledged with gratitude. GNP and TWK are grateful for support from the Korea Science and Engineering Foundation through the Quantum-functional Semiconductor Research Center at Dongguk University. ANB and GNP have been receiving support from the 'Rosnauka' under the project 'IN-12.5/002', which is acknowledged with gratitude.

References

[1] Hummer K 1973 *Phys. Status Solidi* b **56** 249
[2] Ohtomo A, Kawasaki M, Koida T, Masubuchi K, Koinuma H, Sakurai Y, Yoshida Y, Yasuda T and Segawa Y 1998 *Appl. Phys. Lett.* **72** 2466
[3] Sharma A K, Narayan J, Muth J F, Teng C W, Jin C, Kvit A, Kolbas R M and Holland O W 1999 *Appl. Phys. Lett.* **75** 3327
[4] Park W I, Yi G-C and Jang H M 2001 *Appl. Phys. Lett.* **79** 2022
[5] Naryana J, Sharma A K, Kvit A, Jin C, Muth J F and Holland O W 2002 *Solid State Commun.* **121** 9
[6] Choopun S, Vispute R D, Yang W, Sharma R P, Venkatesan T and Shen H 2002 *Appl. Phys. Lett.* **80** 1529
[7] Takeuchi I, Yang W, Chang K-S, Aronova M A, Venkatesan T, Vispute R D and Bendersky L A 2003 *J. Appl. Phys.* **94** 7336
[8] Bhattacharya P, Das R R and Katiyar R S 2004 *Thin Solid Films* **447/448** 564
[9] Chen N B, Wu H Z, Qiu D J, Xu T N, Chen J and Shen W Z 2004 *J. Phys.: Condens. Matter* **16** 2973
[10] Gruber Th, Kirchner C, Kling R, Reuss F and Waag A 2004 *Appl. Phys. Lett.* **84** 5359
[11] Takagi T, Tanaka H, Fujita S and Fujita S 2003 *Japan. J. Appl. Phys.* **42** L401
[12] Kunisu M, Tanaka I, Yamamoto T, Suga T and Mizoguchi T 2004 *J. Phys.: Condens. Matter* **16** 3801
[13] Kondrashev Yu D and Omelchenko Yu A 1964 *Zh. Neorg. Khim. (Rus.)* **9** 937
[14] Segnit E R and Holland A E 1965 *J. Am. Ceram. Soc.* **48** 409
[15] Raghavan S, Hajra J P, Iyengar G N K and Abraham K P 1991 *Thermochim. Acta* **189** 151
[16] Chen J, Shen W Z, Chen N B, Qiu D J and Wu H Z 2003 *J. Phys.: Condens. Matter* **15** L475
[17] Tomar M S, Melgarejo R, Dobal P S and Katiyar R S 2001 *J. Mater. Res.* **16** 903
[18] Jayaram V and Rani B S 2001 *Mater. Sci. Eng.* A **304–306** 800
[19] Bates C H, White W B and Roy R 1962 *Science* **137** 993
[20] Gerward L and Olsen J S 1995 *J. Synchrotron Radiat.* **2** 233
[21] Recio J M, Blanco M A, Luana V, Pandey R, Gerward L and Olsen J S 1998 *Phys. Rev.* B **58** 8949
[22] Desgreniers S 1998 *Phys. Rev.* B **58** 14102
[23] Kusaba K, Syono Y and Kikegawa T 1999 *Proc. Japan Acad.* B **75** 1
[24] Decremps F, Zhang J and Liebermann R C 2000 *Europhys. Lett.* **51** 268
[25] Jiang J Z, Olsen J S, Gerward L, Frost D, Rubie D and Peyronneau J 2000 *Europhys. Lett.* **50** 48
[26] Decremps F, Pellicer-Porres J, Datchi F, Itie J P, Polian A, Baudelet F and Jiang J Z 2002 *Appl. Phys. Lett.* **81** 4820
[27] Karzel H, Potzel W, Kofferlein M, Schiessl W, Steiner M, Hiller U, Kalvius G M, Mitchell D W, Das T P, Blaha P, Schwarz K and Pasternak M P 1996 *Phys. Rev.* B **53** 11425
[28] Mang A, Reimann K and Rubenacke St 1995 *Solid State Commun.* **94** 251
[29] Decremps F, Pellicer-Porres J, Saitta A M, Chervin J-C and Polian A 2002 *Phys. Rev.* B **65** 092101
[30] Segura A, Sans J A, Manjon F J, Munoz A and Herrera-Cabrera M J 2003 *Appl. Phys. Lett.* **83** 278
[31] Jaffe J E, Snyder J A, Lin Z and Hess A C 2000 *Phys. Rev.* B **62** 1660
[32] Sans J A and Segura A 2004 *High Pressure Res.* **24** 119
[33] Larson A C and Von Dreele R B 1994 General Structure Analysis System (GSAS) *Los Alamos National Laboratory Report* LAUR 86-748
[34] Toby B H 2001 *J. Appl. Crystallogr.* **34** 210
[35] Desgranges L, Calvarin G and Chevrier G 1996 *Acta Crystallogr.* B **52** 82
[36] Panin G N, Baranov A N, Oh Y-J and Kang T W 2004 *Curr. Appl. Phys.* **4** 647
[37] Guha S 1980 *Phys. Rev.* B **21** 5808
[38] Vanheusden K, Seager C H, Warren W L, Tallant D R and Voigt J A 1996 *Appl. Phys. Lett.* **68** 403
[39] Egelhaaf H J and Oelkrug D 1996 *J. Cryst. Growth* **161** 190
[40] Kureja L M, Barik S and Misra P 2004 *J. Cryst. Growth* **268** 531